Inorganic Chemistry

Forum Article

pubs.acs.org/IC

Bimetallic Cobalt−Dinitrogen Complexes: Impact of the Supporting Metal on N_2 Activation

Laura J. Clouston, Varinia Bernales, Rebecca K. Carlson, Laura Gagliardi,* and Connie C. Lu*

Department of Chemistry, Supercomputing Institute, and Chemical Theory Center, University of Minnesota, 207 Pleasant Street SE, Minneapolis, Minnesota 55455-0431, United States

Supporting Information

ABSTRACT: Expanding a family of cobalt bimetallic complexes, we report the synthesis of the Ti(III) metalloligand, Ti[N(*o*-(NCH$_2$P(^{i}Pr)$_2$)C$_6$H$_4$)$_3$] (abbreviated as TiL), and three heterobimetallics that pair cobalt with an early transition metal ion: CoTiL (**1**), K(crypt-222)[(N_2)CoVL] (**2**), and K(crypt-222)[(N_2)CoCrL] (**3**). The latter two complexes, along with previously reported K(crypt-222)[(N_2)CoAlL] and K(crypt-222)[(N_2)Co_2L], constitute an isostructural series of cobalt bimetallics that bind dinitrogen in an end-on fashion, i.e. $[(N_2)CoML]^-$. The characterization of **1**−**3** includes cyclic voltammetry, X-ray crystallography, and infrared spectroscopy. The $[CoTiL]^{0/-}$ reduction potential is extremely negative at −3.20 V versus Fc^+/Fc. In the CoML series where M is a transition metal, the reduction potentials shift anodically as M is varied across the first-row period. Among the $[(N_2)CoML]^-$ compounds, the dinitrogen ligand is weakly activated, as evidenced by N−N bond lengths between 1.110(8) and 1.135(4) Å and by N−N stretching frequencies between 1971 and 1995 cm^{-1}. Though changes in ν_{N_2} are subtle, the extent of N_2 activation decreases across the first-row period. A correlation is found between the $[CoML]^{0/-}$ reduction potentials and N_2 activation, where the more cathodic potentials correspond to lower N−N frequencies. Theoretical calculations of the $[(N_2)CoML]^-$ complexes reveal important variations in the electronic structure and Co−M interactions, which depend on the exact nature of the supporting metal ion, M.

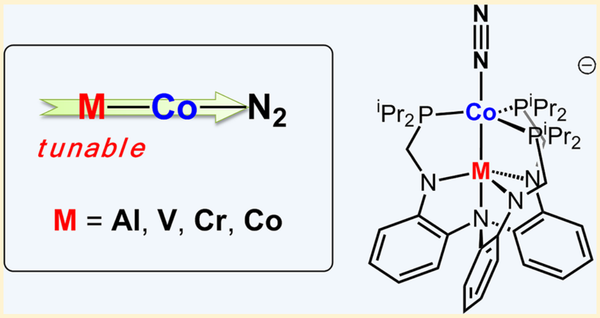

INTRODUCTION

Cobalt is generally surpassed by iron as the choice first-row metal for N_2 activation. In synthetic systems where both cobalt-dinitrogen and iron-dinitrogen adducts are known, the cobalt counterparts typically activate N_2 more weakly.[1−16] This has been attributed to the energetically lower Co d orbitals being worse at π-back-bonding to the N_2 substrate.[17] Nonetheless, the N_2-coordination chemistry at cobalt is substantial, as shown in Figure 1.[1,3,5,7,10,18−21] Included in these examples are the few exceptional cases where cobalt site(s) reduce N_2 by two or more electrons. The cobalt tri(phosphino)borate complex (Figure 1B) mediates an overall two-electron transformation of N_2 to the diazenido species, Co−N═NR.[7] Cobalt diketiminate complexes, when subjected to alkali metals, capture N_2 within a Co−N═N−Co linkage, representing a formal two-electron reduction of N_2 (Figure 1A).[5]

Of relevance, monocobalt and dicobalt complexes have been discovered to catalyze the silylation of N_2 to two $N(SiMe_3)_3$ molecules in a six-electron redox reaction.[22] The dicobalt system features a metal−metal interaction in the precatalyst. Using hemilabile interactions between a catalytic metal center and an ancillary main group ion is a powerful strategy in small-molecule activation.[11,12] An enlightening example is the iron-boratrane system that mediates the reduction of N_2 to NH_3 with seven turnovers at ambient temperature and pressure.[13,14] Recently, the cobalt-boratrane congener (Figure 1E) was shown to be competent in fixing N_2 to NH_3 with 2.4 turnovers.[20] The flexibility of the Co−B interaction was further reinforced as an important factor, as the cobalt complexes of the analogous C and Si ligands were essentially incompetent in the catalysis.

Also of relevance, the ZrCo heterobimetallic system (Figure 1D) harnesses early-late transition metal cooperativity to completely rupture strong C═O bonds in CO_2 and benzophenone in a stoichiometric manner.[23,24] Cleavage of C═O bonds is inherent in the reactivity of a related TiCo complex, which reductively couples aryl ketones to alkenes.[25] Metal cooperativity also operates in triiron platforms that mediate the multielectron reduction and N═N cleavage of azobenzene.[26]

We have been targeting a family of CoM bimetallics to understand how an ancillary metal tunes the Co−M interaction and the overall properties of the bimetallic complex.[15,16,27,28] Reduction of the CoM bimetallics provided access to four

Special Issue: Small Molecule Activation: From Biological Principles to Energy Applications

Received: April 30, 2015
Published: July 1, 2015

DOI: 10.1021/acs.inorgchem.5b00983
Inorg. Chem. 2015, 54, 9263−9270

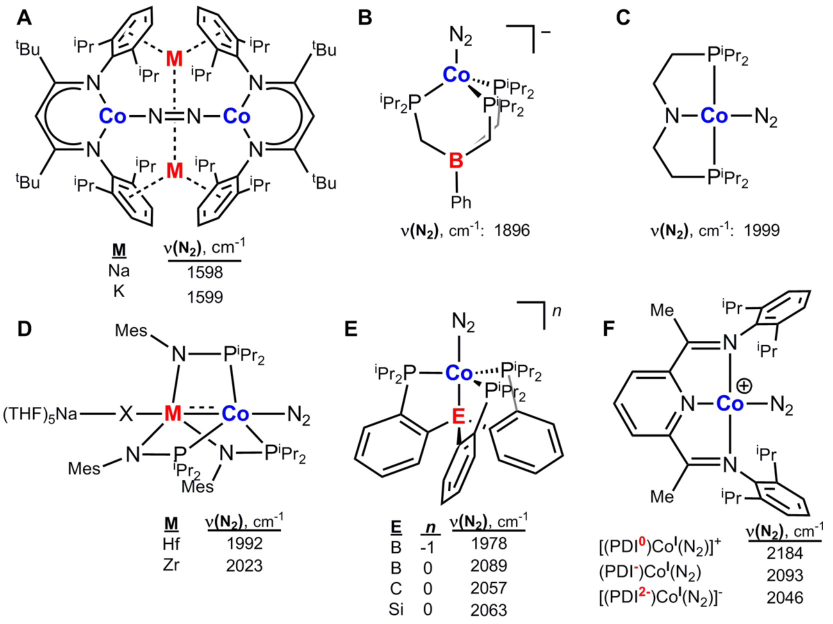

Figure 1. Selected examples of cobalt-dinitrogen complexes from the literature that showcase N_2 activation and tuning of the metal countercation, ligand oxidation state, and ancilliary element.

cobalt-dinitrogen complexes, which are isostructural and showcase tunability of the supporting metal ion. Through synthesis, physical/spectroscopic characterization, and theoretical calculations, we unravel the impact of the ancillary metal on N_2 activation in these cobalt bimetallics.

EXPERIMENTAL SECTION

General Considerations. Unless otherwise stated, all manipulations were performed under an inert atmosphere in a glovebox or using standard Schlenk techniques. Standard solvents were deoxygenated by sparging with inert gas and dried by passing through activated alumina columns of a SG Water solvent purification system. Deuterated solvents were purchased from Cambridge Isotope Laboratories, Inc. or Sigma-Aldrich, degassed via freeze−pump−thaw cycles and stored over activated 4 Å molecular sieves. Elemental analyses were performed by Complete Analysis Laboratories, Inc. (Parsippany, NJ) or Robertson Microlit Laboraties, Inc. (Ledgewood, NJ). ^{1}H NMR spectra were recorded on a Varian 300 MHz or a Bruker 500 MHz spectrometer at ambient temperature unless otherwise stated. Solution magnetic moments were determined using Evans' method.[29,30] Cyclic voltammetry was performed using a CH instruments 600 electrochemical analyzer. The one-cell setup used a glassy carbon working electrode, Pt wire counter electrode, and Ag/$AgNO_3$ reference electrode in CH_3CN. Analyte solutions consisted of 0.4 M [^{n}Bu$_4$N]PF$_6$ and the voltammograms were referenced internally to the FeCp$_2$$^{0/+}$ (abbreviated as Fc$^+$/Fc) redox couple. The ligand N(*o*-(NHCH$_2$P^{i}Pr$_2$)C$_6$H$_4$)$_3$ (abbreviated as H$_3$L), CoVL, and CoCrL were synthesized according to literature procedures.[15,27,28]

Synthesis of Ti(N(*o*-(NCH$_2$P^{i}Pr$_2$)C$_6$H$_4$)$_3$). A solution of neutral ligand (N(*o*-(NHCH$_2$P^{i}Pr$_2$)C$_6$H$_4$)$_3$ (0.308 g, 0.453 mmol) in Et$_2$O (5 mL) was frozen in an LN$_2$ coldwell. The solid was layered with ^{n}BuLi (0.560 mL, 1.40 mmol), and the mixture was allowed to thaw overnight. The volatiles of the resulting yellow solution were removed *in vacuo*. The resulting yellow oil was taken up in THF (5 mL) and frozen in a LN$_2$ cold well along with a solution of TiCl$_3$(THF)$_3$ (0.168 g, 0.454 mmol) in THF (5 mL). The thawing yellow solution of deprotonated ligand was layered on top of the frozen solution of TiCl$_3$(THF)$_3$ and allowed to warm to toom temperature. The solution was allowed to stir for 3 h to yield a brown solution. The reaction was dried *in vacuo* and reconstituted in benzene. The benzene solution was filtered through a Celite pad and dried *in vacuo*, resulting in a brown powder (0.320 g, 97% yield). ^{1}H NMR (ppm, C$_6$D$_6$, 500 mHz): 8.5, 6.2, 5.0, 1.9, 1.0, −2.7. Anal. Calcd for TiL, C$_{39}$H$_{60}$N$_4$P$_3$Ti: 64.55 C, 8.33 H, 7.72 N. Found: 64.09 C, 8.12 H, 7.44 N.

Synthesis of 1 CoTi(N(o-(NCH$_2$P^{i}Pr$_2$)C$_6$H$_4$)$_3$). A solution of TiL (0.174 g, 0.238 mmol) in THF (4 mL) was added to a slurry of CoBr$_2$ (0.0522 g, 0.237 mmol) in THF (2 mL) while stirring. After 15 min, a homogeneous, dark green-brown solution formed, and the solution was added to KC$_8$ (0.0658 g, 0.487 mmol). The green color disappeared within minutes, and the reaction was stirred for an additional 4 h. The reaction solution was filtered through a Celite pad, and the volatiles were removed *in vacuo*. The brown powder was reconstituted in benzene and filtered through a Celite pad to remove salts. The resulting brown solution was dried *in vacuo* to give a brown powder (0.175 g, 93% yield). Single crystals were grown through the slow dissipation of pentane into a concentrated toluene solution. ^{1}H NMR (ppm, THF-*d*$_8$, 500 MHz): 6.80 (*t*, *J* = 7.7 Hz, 3H), 6.71 (*d*, *J* = 7.7 Hz, 3H), 6.16 (*d*, *J* = 7.7 Hz, 3H), 6.12 (*t*, *J* = 7.2 Hz, 3H), 5.28 (*d*, *J* = 11.5 Hz, 3H), 4.53 (*d*, *J* = 11.4, 3H), 2.96 (*s*, 3H), 2.77 (*s*, 3H), 1.60 (*s*, 9H), 1.46 (*s*, 9H), 1.34 (*s*, 9H), 0.53 (*s*, 9H). ^{31}P NMR (ppm, THF-*d*$_8$, 200 MHz): 17.1. ^{13}C NMR (ppm, THF-*d*$_8$, 126 MHz): 156.2, 138.2, 128.4, 126.9, 114.4, 108.0, 68.9, 33.35, 28.53, 23.16, 20.26, 19.53, 17.84. Anal. Calcd for **1** C$_{39}$H$_{60}$N$_4$P$_3$TiCo: 59.70 C, 7.71 H, 7.14 N. Found: 59.82 C, 8.04 H, 6.74 N.

Synthesis of 2 K(crypt-222)[(N$_2$)CoVL], K(C$_{18}$H$_{36}$N$_2$O$_6$)[(N$_2$)-CoV(N(o-(NCH$_2$P^{i}Pr$_2$)C$_6$H$_4$)$_3$)]. A solution of CoVL (0.0817 g, 0.104 mmol) in THF (8 mL) was added to a vial containing KC$_8$ (0.0293 g, 0.217 mmol). A solution of crypt-222 (0.402 g, 0.107 mmol) in THF (4 mL) was added to the stirring reaction mixture and was allowed to stir for 16 h. The resulting brown solution was filtered through a Celite plug to remove graphite, and the volatiles were removed *in vacuo*. The resulting brown powder was washed with 5 × 5 mL portions of benzene and then dried to obtain a brown powder (0.113 g, 89% yield). Single crystals were grown through the layering of a THF solution with hexane. ^{1}H NMR (ppm, THF-*d*$_8$, 500 MHz): 27.1, 12.3, 8.7, 5.5, 3.4, 2.4, 1.3, 0.9, −27.5. Evans' method (THF-*d*$_8$): $\mu_{\text{eff}} = 2.68$ μ_B. IR ($\nu_{\text{N−N}}$, cm^{-1}, KBr pellet): 1971. Anal. Calcd for **2** C$_{57}$H$_{96}$CoVKN$_8$O$_6$P$_3$: 55.60 C, 7.86 H, 9.1 N. Found: 55.99 C, 8.51 H, 7.41 N, and 55.67 C, 7.88 H, 7.64 N for two independent samples. Note: Partial N$_2$ loss during the combustion procedure may account for the low N%.

Synthesis of 3 K(crypt-222)[(N$_2$)CoCrL], K(C$_{18}$H$_{36}$N$_2$O$_6$)[(N$_2$)-CoCr(N(o-(NCH$_2$P^{i}Pr$_2$)C$_6$H$_4$)$_3$)]. THF (6 mL) was added to CoCrL (0.104 g, 0.132 mmol), and the solution was transferred to a slurry of KC$_8$ (0.019 g, 0.138 mmol). The mixture was allowed to stir for 4 h,

Table 1. Crystallographic Details for Compounds 1−3

	1	2	3
chemical formula	$C_{39}H_{60}N_4P_3TiCo$	$C_{39}H_{60}N_6P_3VCo{\cdot}KC_{18}H_{36}N_2O_6{\cdot}C_4H_8O$	$2(C_{39}H_{60}N_6P_3CrCo){\cdot}2(KC_{18}H_{36}N_2O_6)$
fw	784.65	1303.4	2464.7
cryst syst	monoclinic	orthorhombic	monoclinic
space group	$P2_1/n$	$Pna2_1$	$P2_1$
a (Å)	13.5781(18)	63.552(2)	11.2453(3)
b (Å)	13.9450(18)	11.0817(4)	31.9918(7)
c (Å)	20.821(3)	18.9917(7)	18.9780(4)
α (deg)	90	90	90
β (deg)	94.250(2)	90	95.0420(10)
γ (deg)	90	90	90
V (Å^3)	3931.5(9)	13375.2(8)	6801.1(3)
Z	4	8	2
D_{calcd} (g cm^{-3})	1.326	1.295	1.204
λ (Å), μ (mm^{-1})	0.71073, 0.780	1.54178, 4.785	1.54178, 4.831
T (K)	173(2)	123(2)	173(2)
θ range (deg)	1.73−27.50	2.71−74.71	2.337−74.662
reflns collected	9018	25425	27151
unique reflns	5711	22340	23744
data/restraint/params	9018/0/445	25425/1/1476	27151/8/1428
R1, wR2 ($I > 2\sigma(I)$)	0.0527, 0.1170	0.0440, 0.1054	0.0470, 0.1130

and the remaining graphite was filtered off through a Celite plug. The remaining red-brown solution was dried *in vacuo*. The solid was taken up in THF (2 mL) and added to a stirring solution of crypt-222 in THF (6 mL) and allowed to stir for 1 h. The solution was dried *in vacuo* to give a dark powder (0.140 g, 88% yield). Single crystals were grown via the slow diffusion of pentane into a concentrated THF solution. ^{1}H NMR (ppm, THF-d_8, 300 MHz): 15.8, 8.3, 6.5, −21.3. Evans' method (THF-d_8): μ_{eff} = 3.58 μ_B. IR (ν_{N-N}, cm^{-1}, KBr pellet): 1990. Anal. Calcd for **3** $C_{57}H_{96}CoCrKN_8O_6P_3$: 55.55 C, 7.85 H, 9.09 N. Found: 56.86 C, 8.11 H, 6.89 N, which is consistent with K(crypt-222)[CoCrL], $C_{57}H_{96}CoCrKN_6O_6P_3$: 56.84 C, 8.03 H, 6.98 N.

■ X-RAY CRYSTALLOGRAPHY AND STRUCTURE REFINEMENT DETAILS

A brown block of **1**, a brown needle of **2**, and a brown needle of **3** were placed on the tip of a 0.1 mm diameter glass capillary and mounted on a Bruker APEX II CCD diffractometer or a Bruker Photon 100 CMOS diffractometer for data collection at 173(2) K or 123(2) K. The data collection was carried out using Mo Kα radiation (graphite monochromator) or Cu Kα radiation (normal parabolic mirrors).[31] The data intensity was corrected for absorption and decay (SADABS). Final cell constants were obtained from least-squares fits of all measured reflections, and the structure was solved using SHELXS-08 and refined using SHELXL-08.[32] A direct-methods solution was calculated which provided most non-hydrogen atoms from the E-map. Full-matrix least-squares/difference Fourier cycles were performed to locate the remaining non-hydrogen atoms, and all non-hydrogen atoms were refined with anisotropic displacement parameters, with the exception of a disordered THF molecule in **2** which is refined isotropically. Hydrogen atoms were placed in ideal positions and refined as riding atoms with relative isotropic displacement parameters. Complex **3** was refined as an inversion twin with the main component contributing 54%. A disordered isopropyl group in **3** was modeled using SHELXTL EADP constraints and the geometrical restraints SAME and SADI. Electron density attributed to two disordered molecules of pentane in the asymmetric unit was removed using Platon SQUEEZE.[33] Crystallographic details are summarized in Table 1.

■ COMPUTATIONAL METHODS

DFT Calculations. DFT calculations were performed on the full molecules, CoTiL and [(N_2)CoML]$^-$ (where M = Al, Ti, V, Cr, Co). Gas-phase optimizations of all possible spin states were carried out using the M06-L[34] functional and def2-TZVP[35] (for N, P, Al, Ti, V, Cr, and Co atoms)/def2-SVP (for C, H atoms) basis sets. The experimental structures were used as initial geometries. In one case, CoTiL, the optimized Co−Ti distance did not match well to experimental data (both M06-L and PBE underestimated by ∼0.14 Å), so the Co−Ti bond distance was kept fixed, while the rest of the molecule was allowed to relax. Vibrational frequency analysis with the harmonic approximation was performed at the optimized geometries to characterize the nature of the stationary points on the potential energy surface. Gibbs free energies at 298.15 K were computed by adding zero-point vibrational energies, and thermal vibrational−rotational entropy in the quasi-harmonic approximation calculated at the M06-L/def2-TZVP (for N, P, Al, Ti, V, Cr and Co)/def2-SVP(for C, H) level. Solvation effects were also considered by performing single-point calculations for all intermediates using the SMD solvation model[36] with the diffuse basis set, def2-TZVPD[37] (for N, P, Al, Ti, V, Cr, and Co; def2-SVP for C and H) and THF as the solvent. In summary, the energies of all calculated structures were determined at the M06-L/def2-TZVP and M06-L/def2-TZVPD/SMD levels of theory, where the former is used for geometry optimizations and the latter for single-point energy calculations. The *Gaussian 09* suite of programs[38] was used for all DFT calculations. Additionally, CM5 charges[39,40] was performed for all species (SI Table 9).

Multireference Calculations. Four species, CoTiL^{Me} and [(N_2)-CoML]$^-$ (where M = Ti, V, Cr), were further investigated by multireference calculations using the DFT-optimized geometries in the MOLCAS-7.8 program.[41] (Note: In the single case of CoTiL^{Me}, the ligand's P^{i}Pr$_2$ groups were truncated to PMe$_2$ because previous calculations on neutral CoML^{Me} species also used the truncated ligand.) The complete active space self-consistent field (CASSCF)[42] method was used, followed by multiconfigurational second order perturbation theory, CASPT2.[43] The following relativistic all-electron basis sets were used: ANO-RCC-VTZP for Co, Cr, V, and Ti; ANO-RCC-VDZP for P and N; and ANO-RCC-MB for C and H atoms.[44,45] Scalar relativistic effects were included by using the Douglas−Kroll−Hess Hamiltonian.[46,47] The two-electron integral evaluation was simplified by using the resolution-of-identity (RI)[48] and the Cholesky decomposition technique.[49] To avoid intruder states, an imaginary level shift of 0.2 au was used in the CASPT2 calculations.[50]

DOI: 10.1021/acs.inorgchem.5b00983
Inorg. Chem. 2015, 54, 9263−9270

RESULTS AND DISCUSSION

Synthesis and Characterization of CoTiL (1). The cobalt–titanium complex, CoTiL (**1**), is the latest addition to a growing family of isostructural cobalt bimetallics, where L = $[N(o\text{-}(NCH_2P(^iPr)_2)C_6H_4)_3]^{3-}$. Previously, we reported CoVL,[28] CoCrL,[27] Co_2L,[22] and (N_2)CoAlL,[15] where the latter is the only $(CoM)^{3+}$ example in this ligand scaffold, thus far, to bind N_2 in the apical pocket. Complex **1** was synthesized by mixing $CoBr_2$ and the metalloligand TiL, followed by reduction with 2 equiv of KC_8 (Scheme 1). As complex **1** is (d–d)[10] and diamagnetic, it was characterized by multinuclear NMR spectroscopy. A single ^{31}P signal is observed at 17.1 ppm, suggesting 3-fold symmetry. The ^1H NMR spectrum is consistent with a locked C_3 conformation, where the methylene protons in the ligand arms are diastereotopic, and the diisopropyl phosphine groups are split into two methine and four methyl peaks.

Scheme 1. Synthesis of Compound 1

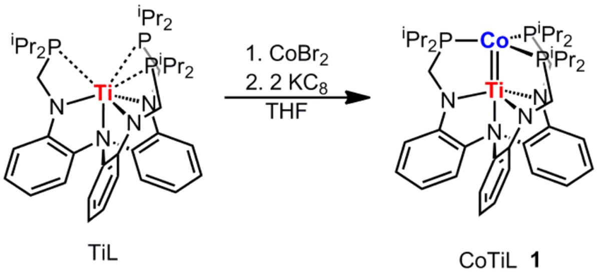

The molecular structure of CoTiL contains a short Co–Ti bond distance of 2.1979(8) Å, which is significantly smaller than the sum of two metals' single-bond radii at 2.48 Å (Figure 2, Table 2).[51] The formal shortness ratio (FSR), the quotient of the metal–metal bond length and the sum of the metals' single-bond radii, is 0.89 for **1**. Of note, it is strikingly longer than the Co–Ti bond length of 2.02 Å in $(PMe_3)Co(^iPr_2PNAr)_2Ti(Cl)$,[25] where the FSR is 0.81 and was interpreted as a Co–Ti triple bond. It is, however, similar to the Co–M bond lengths in the isostructural CoCrL and CoVL compounds (2.14 and 2.12 Å, with FSR values of 0.92 and 0.89, respectively), which were interpreted as Co–M double bonds. By analogy, **1** likely has a Co–Ti double bond.

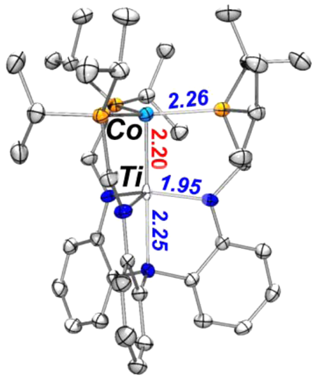

Figure 2. Molecular structure of **1** shown at 50% thermal ellipsoid probability. Hydrogen atoms were omitted for clarity. Average bond lengths (Å) are shown.

Of note, the Co–P bond lengths in CoTiL are similar to those in CoVL, CoCrL, Co_2L, and (N_2)CoAlL, which all fall between 2.21 and 2.30 Å (SI Table 1). For the cobalt-transition metal complexes, the P–Co–P bond angles also adhere to a narrow range of 118–121°. Variation of the supporting metal from Ti to Cr in the amide-binding pocket, hence, has little impact on the ligation of the cobalt in the phosphine pocket. Only (N_2)CoAlL shows a significant distortion from 3-fold symmetry with P–Co–P bond angles of 105, 112, and 132°. The distortion could arise from a Jahn–Teller distortion of a d^9 Co(0) center in 3-fold symmetry.

Electrochemistry of CoML Series. Multiple redox processes have been observed in the cyclic voltammograms (CVs) of the cobalt-transition metal complexes (Figure 3, SI Table 2). The CV of CoTiL (**1**) shows two reversible oxidations at −0.79 and −0.21 V versus Fc^+/Fc. Under argon, a quasi-reversible reduction occurs at −3.20 V, which becomes fully irreversible under N_2. Similar electrochemical behavior was observed for CoVL, CoCrL, and Co_2L, in which the first reductive process is irreversible under N_2 but becomes more reversible under argon.[22,27,28] The behavior is consistent with a rapid chemical reaction, such as N_2 binding, following electron transfer. The (N_2)CoAlL complex has a single, reversible reduction under N_2 at −0.95 V versus Fc^+/Fc. The reversibility is expected as N_2 is already bound to the Co center in (N_2)CoAlL.[15] Of all the cobalt bimetallics, the (N_2)CoAlL has the mildest reduction potential by over 1 V. For the ancillary transition metals, the $[CoML]^{0/-}$ redox potentials become increasingly mild as the supporting metal is varied across the period, i.e. from early to late: CoTiL < CoVL < CoCrL < Co_2L.

Synthesis and Characterization of Dinitrogen Adducts 2 and 3. To probe N_2 activation, chemical reduction of the CoML species with KC_8 followed by addition of crypt-222 provided the end-on N_2 complexes, $[(N_2)CoML]^-$ (Scheme 2). Both K(crypt-222)[(N_2)CoVL] (**2**) and K(crypt-222)[(N_2)CoCrL] (**3**) were successfully generated, but we were unable to isolate any reduced CoTi species. The solution-state magnetic moments of **2** and **3** were measured to be 2.68 and 3.58 μ_B, respectively. Hence, the ground states of **2** and **3** are assigned as $S = 1$ and $S = 3/2$, respectively, as they are close to the spin-only moments of 2.83 and 3.87 μ_B, respectively. The remaining anionic members, $[(N_2)Co_2L]^-$ and $[(N_2)CoAlL]^-$, were reported previously, and are $S = 1$ and $S = 0$, respectively.[16,22]

Figure 4 shows the molecular structures of **2** and **3**. The unit cell for **2** and **3** each contains two unique molecules. The N–N bond elongates upon binding, from 1.098 Å in free N_2 to 1.130(4)/1.135(4) Å and 1.120(7)/1.135(6) Å in **2** and **3**, respectively (Table 2).[52] By this metric, N_2 is slightly less activated in $[(N_2)Co_2L]^-$ and $[(N_2)CoAlL]^-$, which have N–N bond lengths of 1.114(4) and 1.110(8) Å, respectively. Although M–N_2 bond length can be useful to assess metal–N_2 back-bonding, the Co–N bond distances in the $[(N_2)CoML]^-$ complexes are roughly similar, from 1.77 to 1.81 Å (with esd's up to 0.005 Å). Moreover, the Co–N bond in **3** differs by 0.02 Å in the two independent molecules, which also makes it difficult to judge or attribute any subtle differences in Co–N bonds to the supporting metals. Overall, cobalt centers are typically poor at π-back-bonding to N_2, and the N–N and Co–N metrics of these cobalt bimetallics are consistent with weak N_2 activation.

Table 2. Geometrical Parameters, Including Bond Lengths (Å), Formal Shortness Ratio (FSR), and Angles (deg), for 1 − 3, $[(N_2)Co_2L]^-$, and $[(N_2)CoAlL]^-$ (N−N Bond Stretching Frequencies (cm^{-1}) and Reduction Potentials (V vs. Fc^+/Fc) Also Listed)

	1 CoTiL	2^b K(crypt-222)[(N_2)CoVL]		3^b K(crypt-222)[(N_2)CoCrL]		K(crypt-222) [$(N_2)Co_2L$]	K(crypt-222) [(N_2)CoAlL]
Co−M	2.1979(8)	2.6466(7)	2.6661(7)	2.5822(11)	2.5377(12)	2.6771(7)	2.507(2)
FSR[a]	0.89	1.11	1.12	1.11	1.09	1.16	1.02
Co−N		1.796(3)	1.788(3)	1.792(5)	1.813(5)	1.770(4)	1.789(3)
N−N		1.130(4)	1.135(4)	1.135(6)	1.120(7)	1.114(4)	1.110(8)
Co−P	2.2444(11)	2.2024(9)	2.1859(10)	2.1907(15)	2.1988(14)	2.2505(10)	
	2.2553(11)	2.2049(10)	2.1968(10)	2.1918(14)	2.2057(14)	2.2515(10)	2.177(1)
	2.2704(11)	2.2121(10)	2.2094(10)	2.1965(14)	2.2188(15)	2.2651(11)	
M−N_{amide}	1.947(3)	1.952(3)	1.946(3)	1.953(4)	1.975(4)	1.929(3)	
	1.954(3)	1.954(3)	1.949(3)	1.974(4)	1.975(5)	1.931(3)	1.898(3)
	1.955(3)	1.958(3)	1.957(3)	1.980(4)	1.979(4)	1.933(3)	
M−N_{amine}	2.251(3)	2.212(2)	2.222(3)	2.202(4)	2.183(4)	2.135(3)	2.324(6)
Co to P_3−plane	−0.128	0.407	0.428	0.312	0.357	0.383	0.375
M to N_3−plane	0.298	0.356	0.343	0.34	0.328	0.249	0.426
P−Co−P	119.63(4)	109.29(4)	107.59(4)	116.36(6)	122.21(6)	124.02(4)	
	118.16(4)	124.97(4)	121.18(4)	117.64(6)	113.74(6)	112.75(4)	117.10(2)
	121.25(4)	115.63(4)	120.04(4)	120.01(6)	116.31(6)	114.70(4)	
N_{amide}−M−N_{amide}	117.50(13)	117.35(11)	116.39(12)	115.07(18)	118.3(2)	119.01(11)	
	116.68(13)	117.03(11)	118.89(12)	107.07(18)	128.26(19)	118.38(12)	115.11(8)
	118.93(13)	115.89(11)	115.65(12)	128.88(19)	105.13(19)	117.71(12)	
Co−M−N_{amine}	178.90(8)	179.03(7)	178.37(8)	179.06(11)	178.91(12)	178.97(8)	180
M−Co−N		171.11(10)	175.52(10)	176.70(15)	176.60(16)	170.10(11)	180
ν_{N_2} (cm^{-1})		1971		1990		1994	1995
$E°$ $[CoML]^{0/-}$ (V)	−3.20	−2.48		−2.32		−2.11	−0.95

[a] FSR = (Co−M bond distance)/(sum of Co and M single-bond radii).[51] See text. [b] Two unique molecules per asymmetric unit.

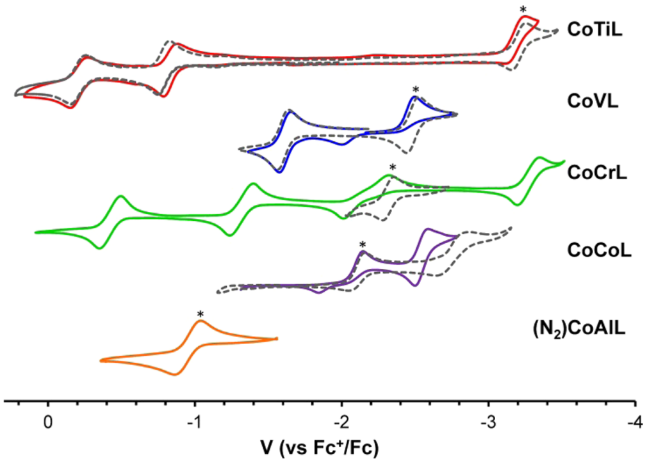

Figure 3. Cyclic voltammograms of CoML and (N_2)CoAlL complexes collected under an atmosphere of N_2 (colored lines) or argon (---) in 0.4 M $[^nBu_4N]PF_6$ in THF at a scan speed of 50 mV/s. Exceptions: 10 mV/s for CoCrL and Co_2L, and the latter was dissolved in 0.1 M $[^nBu_4N]PF_6$ in DME. Asterik (*) marks the $[CoML]^{0/-}$ (or $[(N_2)CoAlL]^{0/-}$) redox couple.

Upon reduction, the FSR values of the Co−M bonds in the cobalt-transition metal pairs all increase above unity (1.1 to 1.2). Presumably, elongation of the Co−M bond is a direct consequence of N_2 binding *trans* to the supporting metal and, thereby, weakening the Co−M interaction. Only $[(N_2)CoAlL]^-$ shows a decrease in FSR (1.06 to 1.02) relative to its neutral analogue (SI Table 1). Again, N_2 already occupies the apical pocket in the neutral complex, and so, the increase in cobalt electron density (by one electron) is interpreted to

Scheme 2. Synthesis of Compounds 2 and 3

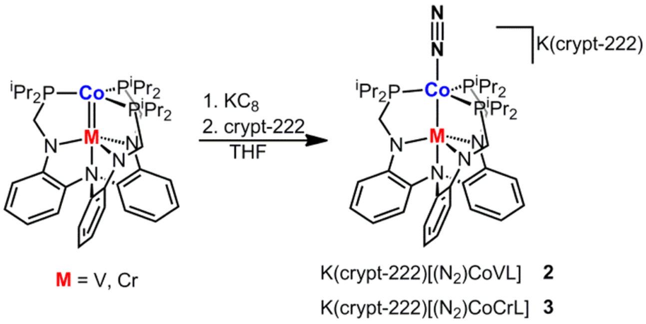

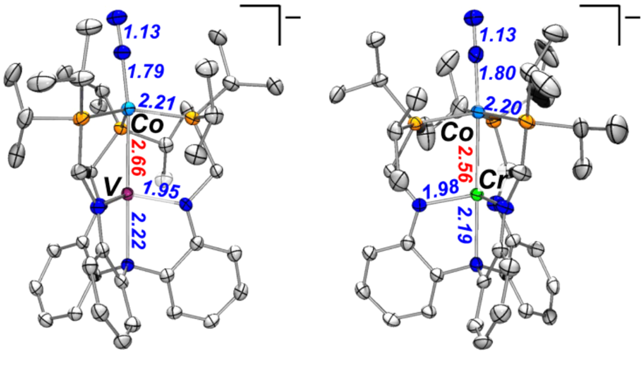

2 3

Figure 4. Molecular structures of 2 and 3 shown at 50% thermal ellipsoid probability. Hydrogen atoms, K(crypt-222) counterion, and noncoordinating solvent molecules were omitted for clarity. Average bond lengths (Å) are shown.

increase cobalt back-bonding to the Lewis acidic Al(III) center. Finally, systematic changes in the Co−P bond lengths can be discerned among the K(crypt-222)[(N_2)CoML] compounds. Specifically, the Co−P bond distances increase according to the order 2.18 Å in [(N_2)CoAlL]$^-$ < 2.19−2.21 in **2** and **3** < 2.26 Å in [(N_2)Co$_2$L]$^-$, where the latter has substantially longer Co−P bonds than the others.

The N−N bond stretching frequency should be a more precise measure of N_2 activation. The N−N frequencies were measured on solid KBr samples of the K(crypt-222)[(N_2)-CoML] complexes. In order of increasing N_2 activation, the frequencies are: 1995 cm^{-1}, [(N_2)CoAlL]$^-$ ≈ 1994 cm^{-1}, [(N_2)Co$_2$L]$^-$ > 1990 cm^{-1}, [(N_2)CoCrL]$^-$ and > 1971 cm^{-1}, [(N_2)CoVL]$^-$.[16,22] The N−N frequencies, which span 24 cm^{-1}, are all consistent with a weakly activated N_2 ligand. Except for a general correlation, we could not pinpoint a precise relationship between the N−N frequencies and the [CoML]$^{0/-}$ reduction potentials, nor alternatively, the E_{pa} of [(N_2)CoML]$^-$. Generally, the N−N frequencies track with the redox potentials for the cobalt-transition metal pairs. For instance, [(N_2)-CoVL]$^-$ and [(N_2)Co$_2$L]$^-$ represent the different extremes of N_2 activation and reducing capability in this series. Dinitrogen is most activated in [(N_2)CoVL]$^-$, and the $E_{1/2}$ of [CoVL]$^{0/-}$ is highly cathodic. The relationship between reducing ability and N_2 activation, however, deteriorates upon inclusion of the Co−Al member. Specifically, N_2 is activated to a similar extent in [(N_2)CoAlL]$^-$ and [(N_2)Co$_2$L]$^-$, though the corresponding [CoML]$^{0/-}$ redox potentials differ by over 1 V.

■ THEORY

The [(N_2)CoML]$^-$ series and CoTiL (**1**) were investigated using density functional theory (DFT) and complete active space self-consistent field (CASSCF) calculations. Optimizations were performed at the DFT level of the [(N_2)CoML]$^-$ anions without truncation for M = Al, Ti, V, Cr, and Co. To model **1**, CoTiL^{Me} (**1′**) was used where P^{i}Pr$_2$ groups were truncated to PMe$_2$ (see Experimental Section). The DFT optimized structures were then used as inputs for multi-configurational CASSCF calculations with second-order perturbation (CASPT2).

The qualitative molecular orbital (MO) diagram of CoTiL^{Me} (**1′**) was identical by DFT and CASSCF methods, and the latter is shown in Figure 5. The main electronic configuration, $\pi^4\sigma^2$(Co 3d$_{xy}$,d$_{x^2-y^2}$)^4, accounts for 83% of the total wave function. To consider the entire ground-state wave function, the occupation numbers were summed over all configurations to give the "total" electronic configuration, $\pi^{3.82}\sigma^{1.89}$(Co 3d$_{xy}$,d$_{x^2-y^2}$)$^{3.88}\sigma^{*0.11}\pi^{*0.18}$(Co 4d$_{xy}$,d$_{x^2-y^2}$)$^{0.12}$. Although the calculations reveal three Co−Ti bonding MOs (σ + 2π), these MOs are quite polarized and cannot be considered as three full bonds. The steep polarization of the σ (Co/Ti: 71/29%) and π MOs (Co/Ti: 86/14% for both) means weakened σ and π bonds, which may be consistent with an experimental FSR that suggests a double Co−Ti bond, rather than triple.

The qualitative splitting diagram for the [(N_2)CoML]$^-$ series is shown in Figure 6. The [(N_2)CoTiL]$^-$ species is purely hypothetical since its experimental congener has not yet been isolated. The energy ordering of the orbitals was based on the DFT calculations. Similar natural orbitals resulted from the CASSCF calculations (SI Figures 8−12), and the polarization of the σ-symmetry MO was obtained from the latter. Across the [(N_2)CoML]$^-$ series, the N_2 π* molecular orbitals are energetically inaccessible, lying well above the HOMO/SOMO for each species. This is consistent with weak N_2 activation and preservation of the N−N triple bond. Of interest, the energy gap between the N_2 π* MOs and the Co d$_{xy}$/d$_{x^2-y^2}$ orbitals remains constant across the different supporting metals, and so, these orbitals were used as a benchmark for comparing Co d-orbital energies.

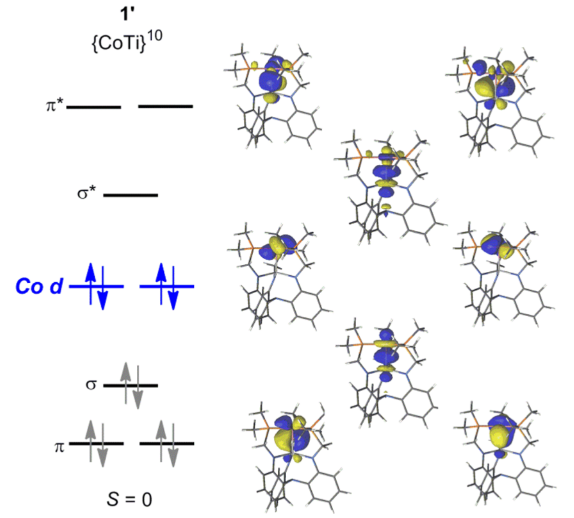

Figure 5. Qualitative MO diagram showing the natural orbitals for CoTiL^{Me} (**1′**) that arise from CASSCF calculations (energy ordering from DFT). The dominating electronic configuration (83%) is shown. The σ/σ* and π/π* labels refer to Co−Ti natural bonding orbitals.

For the transition metal pairings, one notable difference between the [(N_2)CoML]$^-$ anions and their neutral CoML analogues is the greater localization of electrons at the individual metal centers in the anions. Indeed, the only MO with any degree of delocalization is the σ (Co−M). For M = Ti, V, and Cr, the σ (Co−M) is heavily polarized toward cobalt, such that the probability percentages at the two metals, Co and M, are approximately 80 and 20%, respectively. Hence, by DFT, the CoTi, CoV, and CoCr analogues have electronic structures that are approximate to the CoAl species, where the cobalt center is formally subvalent, d^{10} Co(−I), and the supporting metals are trivalent, d^0 Al(III), d^1 Ti(III), d^2 V(III), and d^3 Cr(III). (Note: A detailed CASSCF analysis suggests that the oxidation state of the bimetallic core may be closer to Co(0.5)M(2.5) in the CoTi, CoV, and CoCr species. See SI Table 16.) For M = Ti, V, and Cr, the ligand-field splitting of the cobalt-based d orbitals remains fairly constant for M = Ti, V, and Cr, where the Co d$_{z^2}$ electrons are intermediate in energy between the nonbonding d$_{xz}$/d$_{yz}$ and metal−ligand antibonding d$_{xy}$/d$_{x^2-y^2}$ orbitals. In contrast, the Co d$_{z^2}$ electrons are greatly stabilized by the Lewis acidic Al(III) supporting ion in [(N_2)CoAlL]$^-$.

The dicobalt analogue, [(N_2)Co$_2$L]$^-$, is the stand-out in this series. Unsuprisingly, its electronic structure is different, since it is the only late−late metal pairing. Opposed to the Co(−I)-M(III) redox states of the other anions, the oxidation state of the dicobalt core is Co(0)Co(II). The key difference is the presence of a more delocalized Co−Co σ-bonding MO (63/37%). Hence, a formal single bond is predicted between the two metal centers. The better overlap and mixing between the two metals' d orbitals is likely responsible for the greater ligand-field splitting for the phosphine-ligated cobalt compared to the other anions. Of note, the different oxidation state of Co(0) in the dicobalt anion versus Co(−I) in other [(N_2)CoML]$^-$

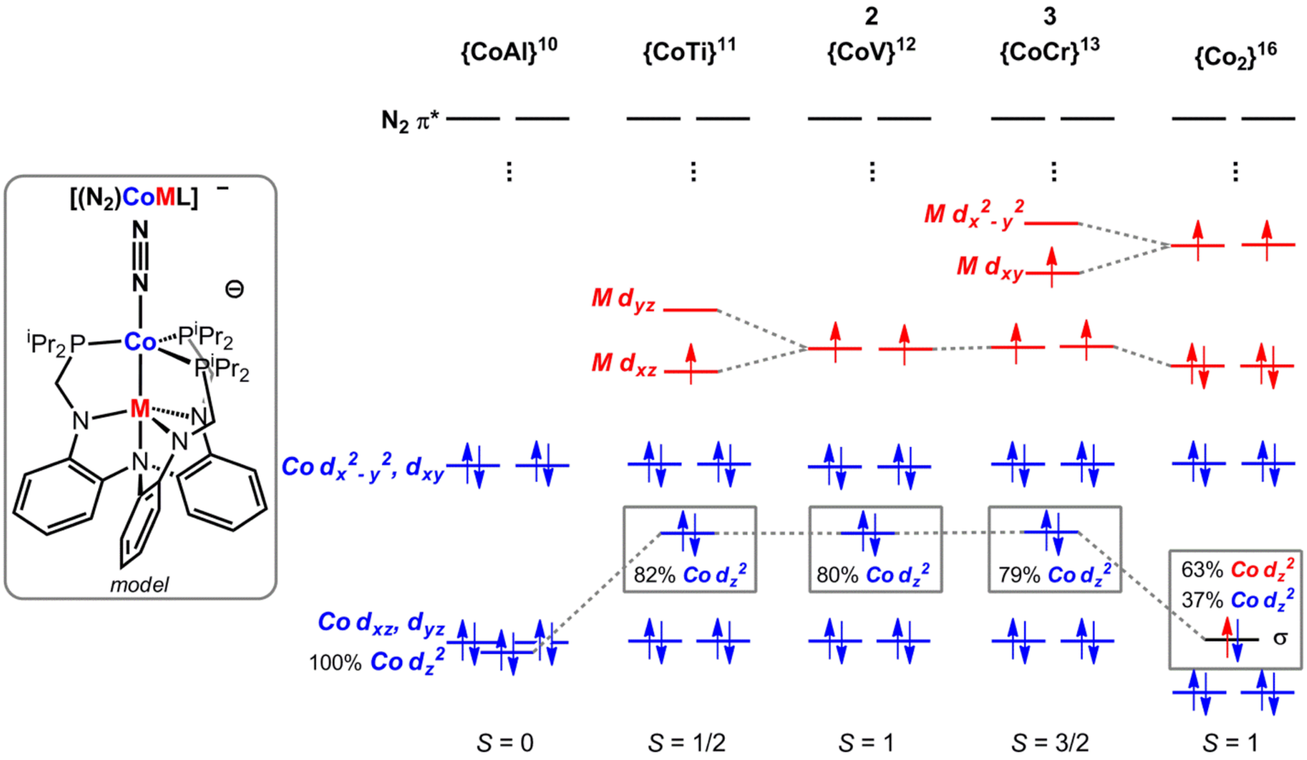

Figure 6. Qualitative MO diagrams of the d-orbital manifold for the $[(N_2)CoML]^-$ series, where M = Al, Ti, V, Cr, and Co. In the $\{CoM\}^n$ descriptor, n is the number of valence d electrons. Polarization of the σ-symmetry MO is given as a percentage.

anions may have observable ramifications. Recall that the Co−P bonds are significantly longer in $[(N_2)Co_2L]^-$ (2.26 Å) compared to the Al, V, and Cr counterparts (2.19−2.21 Å). The shorter Co−P bond lengths in the latter complexes are consistent with a more reduced cobalt site, which can better back-bond to the phosphine ligands.

CONCLUSION

The neutral CoTiL complex is the fifth member of a $(CoM)^{3+}$ family supported by the triphosphino(triamido)amine scaffold. The Co−Ti bond is short at 2.20 Å. Theory predicts three metal−metal bonding MOs ($\sigma + 2\pi$), but the extent of polarization should be taken into account when assigning bond order. Based on a formal shortness ratio of 0.89, we approximate a Co−Ti double bond. Three one-electron transfers are observed in the CV of CoTiL. The $[CoTiL]^{0/-}$ reduction potential is extremely negative at −3.20 V. Including (N_2)CoAlL, the $(CoM)^{+3/+2}$ redox couples in this family span a wide range of 2.25 V. Clearly, the supporting metal ion has a large impact on the $[CoML]^{0/-}$ reduction potentials. Moreover, the $[CoML]^{0/-}$ reduction potentials shift anodically as M is varied across the first-row period.

Of interest to N_2 activation, four isostructural $[(N_2)CoML]^-$ complexes were isolated and characterized for M = Al, V, Cr, and Co.[16,22] The range of N−N bond lengths in the N_2 adducts, $[(N_2)CoML]^-$, is extremely narrow from 1.110(8) to 1.135(4) Å. Likewise, the stretching frequencies of the N_2 adducts span only 24 cm^{-1}. Thus, varying the supporting metal ion has a limited impact on the extent of N_2 activation, perhaps because N_2 binding at the *trans* position tends to weaken the Co−M interaction. Though the changes in ν_{N_2} are subtle, N_2 activation in the $[(N_2)CoML]^-$ series does decrease across the first-row period. As might be expected, there is a general correspondence between the $[CoML]^{0/-}$ reduction potentials ($E^\circ_{1/2}$) and N_2 activation:

$$E^\circ_{1/2}([CoML]^{0/-} \text{ or } [(N_2)CoAlL]^{0/-}):$$

$$\text{Al} \ll \text{Co} < \text{Cr} < \text{V} \ll \text{Ti}$$

$$\nu_{N_2}([(N_2)CoML]^-): \text{Al} \sim \text{Co} > \text{Cr} > \text{V}$$

Varying the supporting metal ion also changes the electronic structure of the $[(N_2)CoML]^-$ species. As elucidated through theory, the oxidation state of the bimetallic $(CoM)^{2+}$ core is Co(−I)M(III) for M = Al, Ti, V, and Cr. The dicobalt anion is unique in that the oxidation states are Co(0)Co(II). The Co−M interactions, which appear similarly weak for M = Ti, V, and Cr, are potentially significant for Al and Co, albeit in different manifestations. In $[(N_2)CoAlL]^-$, an inverse dative bond (Co → Al) greatly stabilizes the Co d_{z^2} electrons, a consequence of pairing cobalt with the Lewis acidic ancillary ion, Al(III). In $[(N_2)Co_2L]^-$, the late−late pairing enables better d-orbital overlap such that a Co−Co σ bond is formed.

ASSOCIATED CONTENT

Ⓢ Supporting Information

Additional experimental and computational data. The Supporting Information is available free of charge on the ACS Publications website at DOI: 10.1021/acs.inorgchem.5b00983. Crystallographic data for **1**−**3** are available through the CCDC 1061357−1061359.

AUTHOR INFORMATION

Corresponding Authors

*E-mail: gagliard@umn.edu.
*E-mail: clu@umn.edu.

Notes

The authors declare no competing financial interest.

■ ACKNOWLEDGMENTS

This experimental work (L.J.C., C.C.L.) was supported by the National Science Foundation (CHE-1254621). The computational work (V.B., R.K.C., L.G.) was supported as part of the Inorganometallic Catalyst Design Center, an EFRC funded by the DOE, Office of Basic Energy Sciences (DE-SC0012702). C.C.L. thanks the Sloan Foundation. L.J.C. was supported by the Graham N. Gleysteen Fellowship in Chemistry. R.K.C. was supported by an NSF graduate fellowship. X-ray diffraction experiments were performed using a crystal diffractometer acquired through an NSF−MRI award (CHE-1229400) in the X-ray laboratory supervised by Dr. Victor G. Young, Jr.

■ REFERENCES

(1) Rozenel, S. S.; Padilla, R.; Arnold, J. *Inorg. Chem.* **2013**, *52*, 11544−11550.

(2) Chomitz, W. A.; Arnold, J. *Chem. Commun.* **2007**, 4797−4799.

(3) Bowman, A. C.; Milsmann, C.; Atienza, C. C. H.; Lobkovsky, E.; Wieghardt, K.; Chirik, P. J. *J. Am. Chem. Soc.* **2010**, *132*, 1676−1684.

(4) Archer, A. M.; Bouwkamp, M. W.; Cortez, M.-P.; Lobkovsky, E.; Chirik, P. J. *Organometallics* **2006**, *25*, 4269−4278.

(5) Ding, K.; Pierpont, A. W.; Brennessel, W. W.; Lukat-Rodgers, G.; Rodgers, K. R.; Cundari, T. R.; Bill, E.; Holland, P. L. *J. Am. Chem. Soc.* **2009**, *131*, 9471−9472.

(6) Smith, J. M.; Lachicotte, R. J.; Pittard, K. A.; Cundari, T. R.; Lukat-Rodgers, G.; Rodgers, K. R.; Holland, P. L. *J. Am. Chem. Soc.* **2001**, *123*, 9222−9223.

(7) Betley, T. A.; Peters, J. C. *J. Am. Chem. Soc.* **2003**, *125*, 10782−10783.

(8) Yu, R. P.; Darmon, J. M.; Milsmann, C.; Margulieux, G. W.; Stieber, S. C. E.; DeBeer, S.; Chirik, P. J. *J. Am. Chem. Soc.* **2013**, *135*, 13168−13184.

(9) Yu, R. P.; Darmon, J. M.; Hoyt, J. M.; Margulieux, G. W.; Turner, Z. R.; Chirik, P. J. *ACS Catal.* **2012**, *2*, 1760−1764.

(10) Whited, M. T.; Mankad, N. P.; Lee, Y.; Oblad, P. F.; Peters, J. C. *Inorg. Chem.* **2009**, *48*, 2507−2517.

(11) Lin, T.-P.; Peters, J. C. *J. Am. Chem. Soc.* **2013**, *135*, 15310−15313.

(12) Lin, T.-P.; Peters, J. C. *J. Am. Chem. Soc.* **2014**, *136*, 13672−13683.

(13) Anderson, J. S.; Rittle, J.; Peters, J. C. *Nature* **2013**, *501*, 84−87.

(14) Moret, M.-E.; Peters, J. C. *Angew. Chem., Int. Ed.* **2011**, *50*, 2063−2067.

(15) Rudd, P. A.; Liu, S.; Gagliardi, L.; Young, V. G.; Lu, C. C. *J. Am. Chem. Soc.* **2011**, *133*, 20724−20727.

(16) Rudd, P. A.; Planas, N.; Bill, E.; Gagliardi, L.; Lu, C. C. *Eur. J. Inorg. Chem.* **2013**, 3898−3906.

(17) Holland, P. L. *Dalton Trans.* **2010**, *39*, 5415−5425.

(18) Greenwood, B. P.; Forman, S. I.; Rowe, G. T.; Chen, C.-H.; Foxman, B. M.; Thomas, C. M. *Inorg. Chem.* **2009**, *48*, 6251−6260.

(19) Setty, V. N.; Zhou, W.; Foxman, B. M.; Thomas, C. M. *Inorg. Chem.* **2011**, *50*, 4647−4655.

(20) Del Castillo, T. J.; Thompson, N. B.; Suess, D. L. M.; Ung, G.; Peters, J. C. *Inorg. Chem.* **2015**, DOI: 10.1021/acs.inorgchem.5b00645

(21) Suess, D. L. M.; Tsay, C.; Peters, J. C. *J. Am. Chem. Soc.* **2012**, *134*, 14158−14164.

(22) (a) Siedschlag, R. B.; Bernales, V.; Vogiatzis, K. D.; Planas, N.; Clouston, L. J.; Bill, E.; Gagliardi, L.; Lu, C. C. *J. Am. Chem. Soc.* **2015**, *137*, 4638−4641. (b) Imayoshi, R.; Tanaka, H.; Matsuo, Y.; Yuki, M.; Nakajima, K.; Yoshizawa, K.; Nishibayashi, Y. *Chem.— Eur. J.* **2015**, *21*, 8905−8909.

(23) Marquard, S. L.; Bezpalko, M. W.; Foxman, B. M.; Thomas, C. M. *J. Am. Chem. Soc.* **2013**, *135*, 6018−6021.

(24) Krogman, J. P.; Bezpalko, M. W.; Foxman, B. M.; Thomas, C. M. *Inorg. Chem.* **2013**, *52*, 3022−3031.

(25) Wu, B.; Bezpalko, M. W.; Foxman, B. M.; Thomas, C. M. *Chem. Sci.* **2015**, *6*, 2044−2049.

(26) Powers, T. M.; Betley, T. A. *J. Am. Chem. Soc.* **2013**, *135*, 12289−12296.

(27) Clouston, L. J.; Siedschlag, R. B.; Rudd, P. A.; Planas, N.; Hu, S.; Miller, A. D.; Gagliardi, L.; Lu, C. C. *J. Am. Chem. Soc.* **2013**, *135*, 13142−13148.

(28) Clouston, L. J.; Bernales, V.; Cammarota, R. C.; Carlson, R. K.; Bill, E.; Gagliardi, L.; Lu, C. C. 2015, in preparation.

(29) Evans, D. F. *J. Chem. Soc.* **1959**, 2003−2005.

(30) Sur, S. K. *J. Magn. Reson.* **1989**, *82*, 169−173.

(31) *Apex2*; Bruker AXS Inc: Madison, WI, 2007.

(32) Sheldrick, G. M. *Acta Crystallogr., Sect. A* **2008**, *64*, 112−122.

(33) Spek, A. L. *Acta Crystallogr., Sect. D: Biol. Crystallogr.* **2009**, *65*, 148−155.

(34) Zhao, Y.; Truhlar, D. G. *J. Chem. Phys.* **2006**, *125*, 194101/1−194101/18.

(35) Weigend, F.; Ahlrichs, R. *Phys. Chem. Chem. Phys.* **2005**, *7*, 3297−3305.

(36) Marenich, A. V.; Cramer, C. J.; Truhlar, D. G. *J. Phys. Chem. B* **2009**, *113*, 6378−6396.

(37) Rappoport, D.; Furche, F. *Chem. Phys.* **2010**, *133*, 134105/1−134105/11.

(38) Frisch, M. J.; Trucks, G. W.; Schlegel, H. B.; Scuseria, G. E.; Robb, M. A.; Cheeseman, J. R.; Scalmani, G.; Barone, V.; Mennucci, B.; Petersson, G. A.; Nakatsuji, H.; Caricato, M.; Li, X.; Hratchian, H. P.; Izmaylov, A. F.; Bloino, J.; Zheng, G.; Sonnenberg, J. L.; Hada, M.; Ehara, M.; Toyota, K.; Fukuda, R.; Hasegawa, J.; Ishida, M.; Nakajima, T.; Honda, Y.; Kitao, O.; Nakai, H.; Vreven, T.; Montgomery, J. A., Jr.; Peralta, J. E.; Ogliaro, F.; Bearpark, M.; Heyd, J. J.; Brothers, E.; Kudin, K. N.; Staroverov, V. N.; Kobayashi, R.; Normand, J.; Raghavachari, K.; Rendell, A.; Burant, J. C.; Iyengar, S. S.; Tomasi, J.; Cossi, M.; Rega, N.; Millam, N. J.; Klene, M.; Knox, J. E.; Cross, J. B.; Bakken, V.; Adamo, C.; Jaramillo, J.; Gomperts, R.; Stratmann, R. E.; Yazyev, O.; Austin, A. J.; Cammi, R.; Pomelli, C.; Ochterski, J. W.; Martin, R. L.; Morokuma, K.; Zakrzewski, V. G.; Voth, G. A.; Salvador, P.; Dannenberg, J. J.; Dapprich, S.; Daniels, A. D.; Farkas, Ö.; Foresman, J. B.; Ortiz, J. V.; Cioslowski, J.; Fox, D. J. *Gaussian 09*, Revision A.1; Gaussian, Inc.: Wallingford, CT, 2009.

(39) Marenich, A. V.; Cramer, C. J.; Truhlar, D. G. *CM5PAC*; University of Minnesota: Minneapolis, MN, 2011.

(40) Marenich, A. V.; Jerome, S. V.; Cramer, C. J.; Truhlar, D. G. *J. Chem. Theory Comput.* **2012**, *8*, 527−541.

(41) Aquilante, F.; De Vico, L.; Ferré, N.; Ghigo, G.; Malmqvist, P.-A.; Neogrády, P.; Pedersen, T. B.; Pitoňák, M.; Reiher, M.; Roos, B. O.; et al. *J. Comput. Chem.* **2010**, *31*, 224−247.

(42) Roos, B. O.; Taylor, P. R.; Siegbahn, E. M. *Chem. Phys.* **1980**, *48*, 157−173.

(43) Andersson, K.; Malmqvist, P. A.; Roos, B. O. *J. Chem. Phys.* **1992**, *96*, 1218−1226.

(44) Roos, B. O.; Lindh, R.; Malmqvist, P.-A.; Veryazov, V.; Widmark, P.-O. *J. Phys. Chem. A* **2004**, *108*, 2851−2858.

(45) Roos, B. O.; Lindh, R.; Malmqvist, P.-A.; Veryazov, V.; Widmark, P.-O. *J. Phys. Chem. A* **2005**, *109*, 6575−6579.

(46) Douglas, M.; Kroll, N. M. *Ann. Phys.* **1974**, *82*, 89−155.

(47) Hess, B. A. *Phys. Rev. A.* **1986**, *33*, 3742−3748.

(48) Vahtras, O.; Almloef, J.; Feyereisen, M. W. *Chem. Phys. Lett.* **1993**, *213*, 514−518.

(49) Aquilante, F.; Lindh, R.; Bondo Pedersen, T. *J. Chem. Phys.* **2007**, *127*, 114107/1−114107/7.

(50) Forsberg, N.; Malmqvist, P.-A. *Chem. Phys. Lett.* **1997**, *274*, 196−204.

(51) Pauling, L. *J. Am. Chem. Soc.* **1947**, *69*, 542−553.

(52) Huber, K. P.; Herzberg, G. *Molecular Spectra and Molecular Structure, 4: Constants of Diatomic Molecules*; Van Nostrand Reinhold: New York, 1979.